Soil moisture mapping in a semiarid region, based on ASAR/Wide Swath satellite data

Mehrez Zribi, Fatma Kotti, Rim Amri, Wolfgang Wagner, Marouen Shabou, Zohra Lili-Chabaane, Nicolas Baghdadi

▶ To cite this version:

Soil moisture mapping in a semi-arid region, based on ASAR/Wide Swath satellite data

M. Zribi[1], F. Kotti[3], R. Amri[13], W. Wagner[2], M.Shabou[13], Z. Lili-Chabaane[3], N. Baghdadi[4]

[1] CESBIO (CNRS/UPS/IRD/CNES), 18 av. Edouard Belin, bpi 2801, 31401 Toulouse cedex 9, France

[2] Institut of Photogrammetry and Remote Sensing, Vienna University of Technology, Vienna, Austria.

[3] INAT-LRSTE/Université de Carthage, 43, Avenue Charles Nicolle 1082 -Tunis- Mahrajène TUNISIE

[4] UMR TETIS, IRSTEA, 500 rue François Breton, 34093 Montpellier cedex 5, France

Abstract

In this paper, an operational algorithm is proposed for the mapping of surface moisture over the northern and central parts of Tunisia, in North Africa. A change detection approach is applied, using 160 multi-incidence Envisat ASAR Wide Swath images acquired in the horizontal polarization over a 7-year period. Parameterization of this algorithm is considered for three classes of vegetation cover density (NDVI<0.25, 0.25<NDVI<0.5 and NDVI>0.5), retrieved from SPOT-VGT decadal images. A relative soil moisture index, ranging between 0 (for the driest surfaces) and 1 (for saturated soils), is proposed for each date, with a resolution of 1 km. The retrieved soil moistures are validated by means of ground measurements based on continuous thetaprobe measurements, as well as low resolution (25 km) ERS and ASCAT soil moisture products from the Vienna University of Technology (TU Wien). A qualitative relationship between spatio-temporal variations of moisture and precipitation is also discussed.

1. Introduction

Soil moisture is a key state parameter of the land surface, influencing the manner in which rainwater is shared between the phenomena of evapotranspiration, infiltration and runoff [Beven et al, 1996; Koster et al, 2004]. In the case of semi-arid regions, this parameter is particularly important for irrigation management [Bastiaanssen et al., 2000]. If water resources, which are often very limited, are to be optimized and protected, an accurate estimation of the soil's water content is needed in order to determine the expected evapotranspiration flux. Considerable efforts have thus been devoted to improving the evaluation of soil moisture and evapotranspiration, and to understanding its relationship with the vegetation cover and the soil's water content [Allen et al., 2005; Albergel et al., 2010].

Radar remote sensing has demonstrated its strong potential for monitoring of soil moistrure over the last twenty years [Ulaby et al., 1996; Wagner et al., 1998; Paloscia et al., 2008; Zribi et al., 2011]. Using Synthetic Aperture Radars (SARs), it is possible to estimate the soil moisture at a high spatial resolution.

The radar signal backscattered by bare soil strongly depends on the soil's moisture content and its surface roughness (e.g. [Fung, 1994]). In the case of sparse vegetation, the return signal depends both on the vegetation's intrinsic backscattering characteristics and on the soil signal attenuation introduced by the vegetation (Bindlish et al., 2001; Zribi et al., 2011, Lievens et al., 2011). Various theoretical and empirical approaches have been developed for bare soils ([Fung, 1994; Oh et al., 2004; Dubois et al., 1995]). Analytical electromagnetic backscatter models (Kirchhoff models, the small perturbation method, and more recently the Integral Equation Model (IEM (Fung et al., 1994), the AIEM (Chen et al., 2003), …) have been used to improve the understanding of radar signal behavior, as a function of surface parameters and soil moisture in particular. In order to reduce the discrepancy between these models and real

data, various improvements have been achieved in the description of roughness (Lievens et al., 2011).

Among these approaches, the "linear approach", which relates the surface soil moisture to calibrated and validated SAR (Synthetic Aperture Radar) measurements expressed in decibels (dB) (SIRC, ERS, RADARSAT, Envisat ASAR, TerraSAR-X...), is widely used (Guerboudi et al., 2011, Moran et al., 2000).

In recent years, different operational algorithms have been proposed, based on a change detection approach. This is particularly relevant for low-resolution spaceborne scatterometers (active microwave) and passive microwave instruments (Njoku et al. 2003, Kerr et al., 2010). The data from scatterometers has been used in a large number of studies related to the study of soil moisture [Wagner et al., 1999, Zribi et al., 2008, Naemi et al., 2009a, Naemi et al., 2009b, Brocca 2011], with the aim of allowing this parameter to be operationally monitored from space, for hydrological or climatic applications (Owe et al., 2008, Albergel et al. 2010, Brocca et al., 2010, Draper et al., 2011). These products would not be sufficient for regional hydrological studies, which require detailed estimations of the spatial variations of soil moisture. In this context, [Wagner et al., 2008; Pathe et al., 2009] proposed a modified approach for the operational estimation of soil moisture at medium spatial resolutions, using the Global and Wide Swath modes of the Advanced Synthetic Aperture Radar (ASAR). [Van Doninck et al., 2012] proposed an adapted algorithmic approach, providing a more accurate analysis of seasonal vegetation effects over Calabria in Italy. The study sites are often in Europe, and often corresponding to humid regions. The major difficulty encountered when applying a change detection algorithm on humid sites is that of under-estimating the radar signal's sensitivity to soil moisture, determined from the difference between the signals acquired for the driest and wettest signals. In practice, it is difficult to retrieve extremely dry

surfaces present in humid regions, when using a limited SAR database for the development of a retrieval algorithm [Hornacek et al., 2012].

In the case of semi-arid regions, seasonal analysis of the influence of vegetation could lead to errors in the estimation of soil moisture. In fact, as a consequence of frequent periods of drought, the dynamics of the vegetation cycle can be highly variable, from one year to another, and even from one period to another within the same agricultural season (Amri et al., 2011). The aim of the present study is thus to apply an operational change detection approach, based on developed methodologies, which takes the particularities of the climate and vegetation cover of semi-arid regions into account. The algorithms proposed in the present study are expected to be highly beneficial for the upcoming SENTINEL-1 mission, for which an operational algorithm will be needed for the mapping of soil moisture. This mission is based on the Sentinel constellation of two C-band radar satellites, of which the first is to be launched in 2013. Given the large data volume generated by Sentinel-1, the techniques developed for the ASAR detection of soil moisture changes are likely to be applicable to, and improved for, this new instrument.

In Section 2, the studied site and database are presented. In Section 3, the algorithm proposed for the estimation of the soil moisture index is presented and validated. Finally, our conclusions are presented in Section 4.

2. Database

2.1 Study area

The study area (Zribi et al., 2011) corresponds to the central and northern parts of Tunisia, situated in North Africa, covering an area approximately 200 km in width and 300 km in length (see Figure 1). The south of the selected site boarders to the Sahara desert, which is of limited interest since it is characterized by extremely low variations in soil moisture. The climate in this region is semi-arid, with an average annual rainfall ranging between

approximately 200 mm per year in the south and 1000 mm per year in the north. It is characterized by a rainy season lasting from October to May, with the two rainiest months being October and March. As is generally the case in semi-arid areas, the rainfall patterns in this area are highly variable in time and space. Figure 1 provides a topographical map of the studied site, whose landscape is nearly flat in the east, and reaches a maximum altitude of 1200 m in the west.

Figure 2 illustrates the land cover of the studied area. The vegetation in the central area is dominated by agriculture (annual crops and arboriculture (mainly olive trees)) and pastures. Various crops are grown and their rotation is typical of semi-arid regions. Cereals are the main annual crop, and sowing generally takes place during the month of December, although this can vary according to the level of precipitation observed during the autumn. The cereals are harvested in the month of June. The north, which is the wettest area, is characterized by the presence of more dense vegetation, in particular the forested zones in the north-west.

Ground measurements

In this section, two types of measurement are considered: moisture and precipitation. Ground moisture measurements were acquired over the last three years (2009-2011), although only in the Kairouan plain in the centre of Tunisia, through the use of two continuous thetaprobe measurements (Amri et al., 2012). All of these measurements are calibrated using gravimetric measurements.

The estimated precipitation levels were based on a network of rain gauges distributed over the entire site. The Inverse Distance Weighting (IDW) interpolation algorithm, widely used in the scientific community, was applied to the recorded data to derive daily precipitation maps. This technique estimates values at non-sampled points, by computing the weighted average of observed data at nearby measurement points. The weighting is defined as a function of the inverse distance of the non-sampled point from each of the neighboring points (Teegavarupu

and Chandramouli, 2005, Shepard et al., 1968). As the landscape is mainly flat in the validation areas, there is no mountainous terrain able to influence the spatial distribution of rainfall.

2.3 Satellite data

a) Envisat ASAR data

The ENVISAT satellite was launched by ESA (European Space Agency) on March 1st, 2002, and was functional until April 8th, 2012. One of its nine Earth-observation instruments, ASAR, was a multi-mode sensor working in the C-band (5.3 GHz), at several polarizations (HH, VV, HV and VH) and at various incidence angles and spatial/radiometric resolutions, depending on its operational mode [Desnos et al., 1999]. At the C-band frequency atmospheric perturbations can be considered to have a negligible influence on the instrumental performance [Ulaby et al., 1981]. The ASAR data used in the present study was provided by ASAR's ScanSAR Wide Swath (WS) observation mode at HH polarization, with a spatial resolution of 150 m and incidence angles ranging between 16 and 43 degrees. Between May 2004 and December 2011, 160 images were acquired at various incidence angles over the central and northern regions of Tunisia. These images cover all four seasons, including dry and wet periods, and were used for the development of the methodology described in the following. Table 1 provides a monthly breakdown of the numbers of images recorded during this period, showing that similar numbers of images was retrieved for all months of the year.

b) SPOT/VGT data

The ten-day synthesis (S10) is a full resolution product (1 km resolution), providing 10-day NDVI (Normalized Difference Vegetation Index) data [Maisongrande et al., 2004]. The NDVI can be related to the green vegetation cover or to the vegetation abundance, and is expressed by: $NDVI = (R_{NIR} - R_{RED})/ (R_{NIR} + R_{RED})$, where R_{NIR} is the near-infrared (NIR)

reflectance and R_{RED} is the red reflectance. The quality of the S10-products is directly related to the quality of the so-called P (physical) products. P products include corrections for atmospheric absorption and scattering, and correspond to top-of-atmosphere (TOA) conditions. The ten-day synthesis products (S10) are available at: http://free.vgt.vito.be/.

c) ERS and ASCAT/METOP moisture products

The ERS and ASCAT/METOP scatterometer radars (active microwave) operate in the C‑band (5.3 GHz), in the vertical polarization. The ERS mission was based on two European Remote Sensing Satellites ERS‑1 (1991–1996) and ERS‑2 (1995 up to 2011). The ASCAT radar is one of the 12 instruments carried by the European Space Agency's METOP-A satellite (launched in 2006). Over land, the measured radar backscattering coefficient depends on the soil moisture, surface roughness, vegetation characteristics, and the incidence angle of the transmitted radar beam. Soil moisture data is retrieved from the backscattering coefficient, through the use of a change detection method developed by the microwave remote sensing team of the Vienna University of Technology (TU Wien), and described by Wagner et al. [1998].

d) SRTM DTM data

The Digital Terrain Model (DTM) provided by the Shuttle Radar Topography Mission (SRTM, http://srtm.usgs.gov/) was used to represent the studied area. The first step involved geo-referencing of the SRTM DTM. The DTM was then re-sampled to the same 1 km resolution as that provided by the radar and SPOT-VGT data. Local slopes were retrieved from the topographic data by computing a simple local derivative, between each pixel and its eight neighboring pixels, at a resolution of 90 m, following which a mean local slope map was computed with a resolution equal to 1 km.

2.4 ASAR data processing

Radar data processing was carried out in three steps:

- Firstly, all images were geo-referenced using a single radar reference image, resulting in an RMS control point error of approximately 0.5 pixel.

- Secondly, all of the images were re-sampled (averaged) to a 1 km resolution. This was needed, to allow the radar data to be compared with SPOT-VGT data, which has a 1 km resolution. A positive side effect of this spatial aggregation is the improved radiometric accuracy of the resulting images.

A mask was developed, to allow cities and high terrain to be eliminated. The cities were retrieved from a classification of LANDSAT images covering the studied area.

Methodology

3.1 Incidence angle normalization

In order to implement a change detection approach, the data must be normalized with respect to the incidence angle under which it is recorded. For the extrapolation of backscatter measurements to a reference angle of 30° a linear model as previously employed by [Wagner et al., 2008, Pathe et al, 2009, Van Doninck et al., 2012] is used:

$$\sigma_0(30°) = \sigma_0(\theta) - \beta(\theta - 30°) \tag{1}$$

where θ is the local incidence angle, σ_0 is the backscattering coefficient in dB, and β is a slope parameter used to normalize the data to a 30° incidence angle. This parameter is very sensitive to the vegetation's characteristics [Wagner et al., 1998, Van Doninck et al., 2012] and to the local topography. For each pixel (x,y) three possible normalizations were thus considered, depending on the vegetation density encountered in this pixel. The S10 SPOT-VGT NDVI database was used to classify the vegetation into one of the following classes:

- Class I, with NDVI<0.25, corresponding to bare soils and/or very sparse vegetation;

- Class II, with 0.25<NDVI<0.5, corresponding to the vegetation encountered during the growing season in annual agricultural areas, and pastures during the wet season:

- Class III, with NDVI>0.5, corresponding to dense vegetation (forests, agricultural areas at their maximum annual growth, …).

These thresholds were selected on an empirical basis, through the analysis of temporal variations of the three dominant forms of vegetation cover (very sparse vegetation, pastures and forests or annual agriculture) over the last 13 years (1998-2011).

For each pixel (x,y), a maximum of three possible radar signal groups, corresponding to the three vegetation classes listed above, are identified in each of the 160 images. For some pixels, for example in forested areas, just one group corresponding to class III was identified. For the other pixels, two or three groups could be identified. For each pixel (x,y), each group includes data belonging to the same vegetation class, but is characterized by different incidence angles from one radar image to the next. This information can then be used to normalize the data with respect to the incidence angle under which it was recorded. In order to ensure good normalization quality, a certain volume of data is needed in each group. Empirically, this quantity was found to be a minimum of 30 data points in each group.

On each radar image, each pixel (x,y) is normalized by the corresponding slope β ($\beta 1$, $\beta 2$, $\beta 3$), which depends on the vegetation density retrieved from the corresponding SPOT-VGT image. Figure 3 shows the mapping of slopes β_1, β_2 and β_3, corresponding to the three vegetation classes I, II and III, computed for the entire studied site. Because of spatial vegetation dynamic variations over the site, the three slopes were not computed for all points on the studied site. The presence of β_1 estimations (black pixels) is limited in the north, since the vegetation is generally dense in this area. Conversely, the values of β_3 corresponding to dense vegetation were not computed in the south, and the β_2 slope was estimated mainly in

the central area. It should be noted that the lowest slope values correspond to the highest vegetation densities observed in the north (approximately 0.05 dB/°), whereas the highest β values (approximately 0.69 dB/°) were retrieved from bare soil in the south. These results are coherent with the trends predicted by bare soil and vegetation backscattering models. It is important to note that, in general, the slope of each pixel is characterized by temporal variability. In fact, the vegetation class of the majority of pixels changes over time, such that the normalized slope β varies throughout the vegetation cycle. For example, for a given pixel, β_1 could be applied during the dry summer season, whereas β_2 or β_3 could be applied at the time of vegetation growth during the rainy season.

Figure 4 illustrates, for the cases of two different pixels, the normalization of multi-incidence data, for different vegetation classes. The first pixel is located in central Tunisia, at a time of the year when there are sparse and medium density vegetation covers, and the second pixel is located in the north, where there are medium and dense vegetation covers. On the first pixel, the slope of the linear fit can be seen to decrease from 0.23dB/° to 0.18dB/°, when the NDVI increases from Class I to Class II, and on the second pixel, the slope also decreases, from 0.19dB/° to 0.16dB/°, when the NDVI increases from Class II to Class III.

3.2 Development of a surface moisture index

A change detection approach, similar to that described in other scientific studies [Wagner et al., 2008, Van Doninck et al., 2012], is proposed here: a relative surface soil moisture index, ranging between 0 and 1 (0 for the driest conditions, 1 for the wettest conditions) is defined for each pixel (x,y) by:

$$I_m(x,y) = \frac{\sigma^0(x,y) - \sigma_i^{dry}(x,y)}{S_i(x,y)} \tag{2}$$

where $S_i(x,y) = \sigma_i^{wet}(x,y) - \sigma_i^{dry}(x,y)$

In the above expression, $\sigma_i^{d\prime}(x,y)$ is the dry reference backscattered signal in dB, at pixel (x,y), for the ith vegetation class (where i = I, II or III). This parameter is defined as the average value of the 5% lowest backscatter coefficients in the Class I time series, and corresponds to the driest conditions for this pixel.

$\sigma_i^{w\prime}(x,y)$ is the wet reference backscattered signal in dB, at pixel (x,y), for the ith vegetation class (where i = I, II, or III). This parameter is defined as the average value of the 5% highest backscatter coefficients in the Class I time series, and corresponds to the wettest conditions for this pixel. By using these average values for the dry and wet radar signals, any noise, which could have a strong influence on the accuracy of moisture estimations, is reduced.

Using 1 km resolution SRTM-processed data, a mask is defined in order to remove from the surface moisture map any areas having local slopes greater than an offset Sl_{max}. In these areas, the moisture estimations could be affected by significant errors, from one image to another, resulting from changes in the satellite's relative viewing angle, and for which it would be difficult to normalize the data with respect to the incidence angle. In order to estimate the most appropriate value for this threshold, the 5% driest images (all of which were recorded during the summer season), corresponding to the lowest backscatter coefficients, were considered. From these images, empirical evaluations showed that all artifacts produced by the slope of the terrain could be eliminated, by applying an offset Sl_{max} equal to approximately 20%.

For each pixel (x,y), $S_i(x,y)$ is the sensitivity of the backscatter coefficient to soil moisture variations, for each vegetation class (I, II or III). The sensitivity is defined as the difference between $\sigma_i^{d\prime}(x,y)$ and $\sigma_i^{w\prime}(x,y)$.

As for the slope maps, the sensitivities were not computed for all pixels on the studied site. S1 was computed mainly in the south, which is characterized by sparse vegetation. S3 was

estimated mainly in the north, which is characterized by the presence of forests and dense annual agriculture. For 6% of the pixels, the sensitivity was computed for all three classes, for 71% of the pixels, the sensitivity was computed for two classes, and for 23% of the pixels, the sensitivity was computed for only one class.

As could be expected, the highest values of sensitivity are observed for bare soils and low dispersion vegetation, and the lowest values of sensitivity are observed for high vegetation densities, with values ranging between 2.8 dB and 14 dB. The proposed semi-arid site is characterized by extremely high variations in soil moisture, i.e. ranging from parched to very wet soil, even during the rainy season. This is mainly due to the frequent occurrence of drought events, which are a climatic characteristic of the Mediterranean climate. In this study, approximately 160 images were considered, distributed over all months of the year, as shown in Table 1. Accurate values of S_i can *a priori* be retrieved, with a limited risk of under-estimation. In the case of humid or extremely dry regions, the soil moisture variations are not necessarily sufficient to cover all of the scenarios encountered in a limited database. For bare soils in the south, S_1 generally lies in the range from 10-14dB. In the case of the forests in the west and the north, the attenuation resulting from the vegetation cover in these areas leads to the smallest S_3 values, i.e. approximately 4-5dB. This is the case for which the soil moisture is estimated with the lowest accuracy.

3.3 Validation of retrieved soil moistures

a) Validation through ground measurements

As described in section 2, ground soil moisture measurements are made only in the Kairouan plain in central Tunisia, such that this is the only part of the studied site for which ground measurement validations could be considered. In order to compare the relative soil moisture index with ground volumetric moisture measurements, the ground measurements were converted to a moisture index through the use of the 90% confidence interval of a Gaussian

distribution [Pellarin et al., 2006], given by $\mu \pm 1.65*\sigma$, where μ and σ are respectively the mean and standard deviation of the thetaprobe ground data:

$$I_m(t) = (\theta(t) - \theta_{min})/(\theta_{max} - \theta_{min}) \qquad (3)$$

where $\theta(t)$ is the soil moisture content at time t [m^3m^{-3}], $I_m(t)$ is the surface soil moisture index at time t, θ_{max} is the maximum wetness value [m^3m^{-3}], equal to ($\mu + 1.65 * \sigma$), and θ_{min} is the minimum wetness value [m^3m^{-3}], equal to ($\mu - 1.65 * \sigma$).

Fig. 5 illustrates the ground surface moisture and precipitation measurements recorded during the study period, from 2009 to 2011, showing high moisture values after heavy rainfall events. The soil moisture can be seen to be highly dynamic, even during the rainy season, due to the high levels of evaporation encountered in this area.

Figure 6 compares the ground measurements acquired using two thetaprobes during the period from 2009 to 2011 with the proposed inversions over two local areas in central Tunisia. Each point on this chart corresponds to a single date, on which ASAR data and ground measurements are compared. The data plotted in Figure 6 is reasonably well correlated (R^2=0.49), and has an RMS error equal to 0.13 (approximately 3.5% as volumetric moisture). Simultaneous satellite acquisitions and ground measurements were recorded on only a small number (27) of dates. The highest value of soil moisture, for which a strong discrepancy was observed between the value retrieved from ASAR (0.91) and that measured on the ground (0.62), was preceded by a small rainfall event some hours before the radar acquisition. This rainfall event would have been sufficient to strongly increase the soil moisture down to a depth of a few millimeters, or perhaps down to one to even two centimeters, but not to the greatest depth of the thetaprobe measurements, which are made between approximately 3 and 7 cm. This discrepancy could thus be explained by the fact that

the C band has a limited penetration depth under wet conditions. This type of scenario arises frequently in semi-arid conditions, as a result of the frequent occurrence of brief rainfall events, combined with a high rate of evaporation, which limits the depth to which the rainwater can infiltrate.

b) Inter-comparison with ERS/ASCAT products

The low resolution ERS and ASCAT products proposed by the Vienna University were validated in Central Tunisia (Kairouan plain) through the use of ground thetaprobe measurements and surface models [Amri et al., 2012, Zribi et al., 2010]. (Amri et al., 2012) showed that there is a good agreement between the satellite and ground estimations acquired over the three-year period from 2009 to 2011, with an rms error equal to 0.043 m^3/m^3 and a correlation coefficient equal to 0.5.

An inter-comparison between the retrieved indices and the scatterometer products (ASCAT and ERS/WSC) was carried out in the present study, for two scatterometer pixels situated in the Kairouan plain. For the ASAR products, a mean value was calculated for each scatterometer pixel. The comparisons were made for dates common to two different types of measurement, thereby limiting the number of illustrated points. Figure 7 shows that the data is in excellent agreement for the two pixels, with a correlation coefficient respectively equal to 0.8 and 0.81, an RMS error equal to 0.13 and 0.087 (approximately 3.5% and 2.3% in terms of volumetric moisture). Only a small difference is observed between the soil moisture algorithms used with the scatterometer and the ASAR WS data, providing complementary confirmation of the product's robustness.

c) Coherence with precipitation levels

In the Kairouan plane, a strong correlation is observed between high moisture values and rainfall, since in 88% of cases for which the retrieved moisture index is higher than 0.4 (corresponding to 14% volumetric moisture), a precipitation event was observed in the five

preceding days. This percentage increases if the number of days preceding the moisture estimation is increased to ten. In approximately 20% of cases for which the moisture index is lower than 0.2 (corresponding to ~7% volumetric moisture), a precipitation event was observed in the five preceding days. This percentage reduces to just 2.5% when precipitation events occurring only two days prior to the moisture estimation are taken into account. These results clearly show that our algorithm reveals a strong correlation between rainfall and the retrieved moisture dynamics.

In the case of the second location, situated near to Béja city in Northwest Tunisia, a strong correlation is also observed between rainfall and the retrieved soil moisture values. In 100% of cases for which the retrieved moisture index was higher than 0.4, a rainfall event had occurred in the five preceding days. Less than 15% of the estimated moisture index values were lower than 0.2, when a rainfall event had occurred in the five preceding days.

d) Analysis of spatio-temporal variations of SM products

Figure 8 shows 1 km resolution soil moisture maps, corresponding to six different dates, indicating generally low values in summer and higher values in winter, which is coherent with the known precipitation trends over this site. These figures are characterized by a high spatial variability of the soil moisture, varying quite strongly from one date to another, as a consequence of localized rainfall events. For example, on 03/11/2010 an increase in soil moisture was observed in the north. This is found to be very well matched with local precipitation events of around 7-10 mm, recorded on the same day, and 5 mm recorded the previous day, whereas no precipitation was recorded in the southern part of the site. The map retrieved for 01/06/2011 indicates a high level of soil moisture in central Tunisia, which is well correlated with two local precipitation events: approximately 8 mm of rain fell the same day, and 1 mm fell the previous day. The map retrieved for 13/01/2009 is also well correlated

with a strong precipitation event (between 14 and 30 mm of rain), which covered the entire studied site on the same day.

4- Conclusions

In this paper, a change detection approach, based on the interpretation of 160 Envisat ASAR WS radar images, is proposed for the operational retrieval of soil moisture over a semi-arid region in North Africa. The backscattered signal, normalized to a 30° incidence angle, was scaled between the lowest and highest values of the studied database. The influence of vegetation, which in these semi-arid regions is characterized by high temporal variations associated with seasonal influences and periods of drought, is taken into account by ranking the radar pixels according to three vegetation classes, through the use of empirical thresholds defined by: NDVI < 0.25, 0.25 < NDVI < 0.5 and NDVI > 0.5. The proposed moisture index was validated firstly through the use of ground measurements recorded in central Tunisia. This comparison revealed an RMS error equal to 0.13 and a correlation coefficient equal to 0.49. The proposed index was then compared with the ERS and ASCAT scatterometer products covering the same area, developed by the Vienna Technical University. The results show that these models are in good agreement, with an RMSE lower than 0.13 and a correlation coefficient equal to 0.8 for two studied pixels. In qualitative terms, there is a high degree of coherence between the estimated moisture dynamics and the observed levels of precipitation, associated with high moisture values. In central Tunisia for example, more than 88% of the estimations with moisture index greater than 0.4 correspond to a precipitation event having occurred in the five previous days. Soil evaporation, an essential parameter in the analysis of the water cycle in semi-arid regions, is estimated using a semi-empirical approach taking soil moisture and the vegetation cover fraction into account. These analyses clearly demonstrate the potential of SENTINE-1 data, when combined with optical data (Sentinel-2 or other products), for the development of operational soil moisture products at a

medium resolution and a high temporal frequency. Such products could be assimilated into various process models and used, in particular, for the development of global evapotranspiration mapping applications.

Acknowledgements

References

Allen, R. G., L. S. Pereira, M. Smith, D. Raes, and J. L. Wright (2005), FAO-56 dual crop coefficient method for estimating evaporation from soil and application extensions, *Journal of Irrigation and Drainage Engineering*, vol. 131, 1(2).

Albergel, C., J.-C. Calvet, P. De Rosnay, G. Balsamo, W. Wagner, S. Hasenauer, V. Naeimi, E. Martin, E. Bazile, F. Bouyssel, and J. F. Mahfouf (2010), Cross-evaluation of modelled and remotely sensed surface soil moisture with in situ data in southwestern France, *Hydrol. Earth Syst. Sci.*, vol. 14, pp. 2177-2191.

Amri, R. M. Zribi, B. Duchemin, Z. Lili-Chabaane, C. Gruhier, A. Chebouni, Analysis of vegetation behaviour in a semi-arid region, using SPOT-VEGETATION NDVI data, *Remote Sensing* , 2011, *3*, 2568-2590.

Amri, R., M. Zribi, Z. Lili-Chabaane, W. Wagner, S. Hauesner (2012), Analysis of ASCAT-C band scatterometer estimations derived over a semi-arid region, *IEEE Trans. Geosci. Remote Sens*, vol. 50, 7, Part I, 2630-2638.

Bastiaanssen, W. G. M., D. J. Molden, and I. W. Makin (2000), Remote sensing for irrigated agriculture: examples from research and possible applications," *Agr. Water Manage*., vol. 46, pp. 137-155.

Beven, K. G., and J. Fisher (1996), Remote Sensing and Scaling in Hydrology, in: Scaling in Hydrology Using Remote Sensing, edited by: Stewart, J. B., Engman, E. T., Feddes, A., and Kerr, Y., Wiley, New York, 93–111.

Bindlish, R., and A. P. Barros (2001), Parameterization of vegetation backscatter in radar-based soil moisture estimation," *Remote Sens. Environ*., vol. 76, pp. 130–137.

Brocca, L., F. Melone, T. Moramarco, W. Wagner, V. Naeimi, Z. Bartalis, and S. Hasenauer (2010), Improving runoff prediction through the assimilation of the ASCAT soil moisture product, *Hydrol. Earth Syst. Sci*., 14, 1881-1893.

Brocca, L., S. Hasenauer, T. Lacava, F. Melone, T. Moramarco, W. Wagner, W. Dorigo, P. Matgen, J. Martines-Fernandez, P. Llorens, J. Latron, C. Martin, and M. Bitelli (2011), Soil moisture estimation through ASCAT and AMSR-E sensors: an intercomparison and validation study across Europe, *Remote Sens. Environ.*, 115, 3390–3408, doi:10.1016/j.rse.2011.08.003.

Chanzy, A., and L. Bruckler (1993), Significance of soil surface moisture with respect to daily bare soil evaporation. *Water Resour. Res..*, 29, 1113–1125.

Chen, K. S., T. D. Wu, L. Tsang, Q. Li, Shi, J., and A. K. Fung (2003), Emission of rough surfaces calculated by the integral equation method with comparison to three-dimensional moment method simulations, *IEEE Trans. Geosci. Remote Sens.*, vol. 41, pp. 90–101.

Desnos, Y. L., H. Laur, P. Lim, P. Meisl, and T. Gach (1999), The ENVISAT-1 Advanced Synthetic aperture radar processor and data products, *Geoscience and Remote Sensing Symposium*, IGARSS'99, Hamburg, Germany, pp. 1683–1685.

Draper, C., J.-F. Mahfouf, J.-C. Calvet, E. Martin, and W. Wagner (2011), Assimilation of ASCAT near-surface soil moisture into the SIM hydrological model over France, *Hydrol. Earth Syst. Sci.*, 15, 3829-3841.

Dubois, P. C., J. Van Zyl, T. Engman (1995), Measuring soil moisture with imaging radars," *IEEE Trans. Geosci. Remote Sens.*, vol. 33, 4, pp. 915–926.

Er-Raki, S., G. Chehbouni, N. Guemouria, B. Duchemin, J. Ezzahar, R. Hadria (2007), Combining FAO-56 model and ground-based remote sensing to estimate water consumptions of wheat crops in a semi-arid region. *Agr. Water Manage.*, 87, 41-54.

Fung, A. K. (1994), Microwave Scattering and Emission Models and their Applications, Artech House.

Gherboudi, I., R. Magagi, A. A. Berg, and B. Toth (2011). Soil moisture retrieval over agricultural fields from multi-polarized and multiangular RADARSAT-2 SAR data, *Remote Sens. Environ.*, 115, 33–43, doi:10.1016/j.rse.2010.07.011.

Hornacek, M., Wagner, W., Sabel, D., Truong, H.L., Snoeij, P., Hahmann, T., Diedrich, E., & Doubkova, M. (2012). Potential for High Resolution Systematic Global Surface Soil Moisture Retrieval via Change Detection Using Sentinel-1. *IEEE Journal of Selected Topics in Applied Earth Observations and Remote Sensing.*

Kerr, Y. H., P. Waldteufel, J. P. Wigneron, S. Delwart, F. Cabot, J. Boutin, M. J. Escorihuela, J. Font, N. Reul, C. Gruhier, S. E. Juglea, M. R. Drinkwater, A. Hahne, M. Martin-Neira, and S. Mecklenburg (2010). The SMOS mission: new tool for monitoring key elements of the global water cycle, P. IEEE, 98, 666–687, doi:10.1109/JPROC.2010.2043032.

Koster, R. D., P. A. Dirmeyer, Z. Guo, G. Bonan, E. Chan, P. Cox, C. T. Gordon, S. Kanae, E. Kowalczyk, D. Lawrence, P. Liu, C. H. Lu, S. Malyshev, B McAvaney, K. Mitchell, D. Mocko, T. Oki, K. Oleson, A. Pitman, Y. C. Sud, C. M. Taylor, D. Verseghy, R. Vasic, Y. Xue, and T. Yamada (2004), Regions of Strong Coupling Between Soil Moisture and Precipitation, *Science*, vol. 305, pp. 1138–1140, doi:10.1126/science.1100217.

Lievens, H. and Verhoest, N. E. C. (2011), On the retrieval of soil moisture in wheat fields from L-band SAR based on water cloud modeling, the IEM and effective roughness parameters, *IEEE Trans. Geosci. Remote Sens.*, 8, 740–744, doi:10.1109/LGRS. 2011.2106109.

Lievens, H., N. E. C. Verhoest, E. De Keyser, H. Vernieuwe, P. Matgen, J. A´lvarez-Mozos, and B. De Baets (2011), Effective roughness modelling as a tool for soil moisture retrieval from C- and L-band SAR, *Hydrol. Earth Syst. Sci.*, 15, 151–162, doi:10.5194/hess-15-151-2011.

Mahfouf, J. F., and J. Noilhan (1991), Comparative study of various formulations of evaporation from bare soil using in situ data. *J. Appl. Meteo Clim*, 30, 1354–1365.

Maisongrande, P., B. Duchemin, and G. Dedieu (2004), « VEGETATION/SPOT—an operational mission for the earth monitoring—presentation of new standard products," *Int. J. Remote Sens*., vol. 25, pp. 9 –14.

Merlin, O., A. Al Bitar, V. Rivalland, P. Beziat, E. Ceschia, G. Dedieu (2011), An analytical model of evaporation efficiency for unsaturated soil surfaces with an arbitrary thickness. *J. Appl. Meteo Clim*. 50 (2), 457–471.

Morana, M. S., D. C. Hymerb, J. Qi, C. Edson E. Sano (2000), Soil moisture evaluation using multi-temporal synthetic aperture radar (SAR) in semiarid rangeland, *Agricultural and Forest Meteorology*, vol. 105, pp. 69–80.

Naeimi, V., Z. Bartalis, and W. Wagner (2009), ASCAT soil moisture: An assessment of the data quality and consistency with the ERS scatterometer heritage, *J. Hydrometeorol.*, vol. 10, no. 2, pp. 555–563.

Naeimi, V., K. Scipal, Z. Bartalis, S. Hasenauer, and W. Wagner (2009), An improved soil moisture retrieval algorithm for ERS and METOP scatterometer observations, *IEEE Trans. Geosci. Remote Sens.*, vol. 47, no. 7, pp. 1999–2013.

Njoku, E. G., T. J. Jackson, V. Lakshmi, T. K. Chan, and S. V. Nghiem (2003), Soil moisture retrieval from AMSR-E, *IEEE Trans. Geosci. Remote Sens*, 41, 215–229, doi:10.1109/TGRS.2002.808243.

Oh, Y. (2004), Quantitative retrieval of soil moisture content and surface roughness from multipolarized radar observations of bare soil surfaces," *IEEE Trans. Geosci. Remote Sens.*, vol. 42, no. 3, pp. 596–601.

Owe, M., R. A. M. De Jeu, and T. R. H. Holmes (2008). Multisensor historical climatology of satellite-derived global land surface moisture, *J. Geophys. Res.*, 113, F01002, doi:10.1029/2007JF000769.

Paloscia, S., P. Pampaloni, S. Pettinato, E. Santi (2008), A Comparison of Algorithms for Retrieving Soil Moisture from ENVISAT/ASAR Images, *IEEE Trans. Geosci. Remote Sens.* vol. 46, 10, pp. 3274-3284.

C. Pathe, W. Wagner, D. M. Doubkova, and J. B. Basara (1999), Using ENVISAT ASAR Global Mode Data for Surface Soil Moisture Retrieval Over Oklahoma, USA, *IEEE Trans. Geosci. Remote Sens*, vol**.** 47, Issue: 2, pp. 468 – 480.

Pellarin, T., J. C. Calvet, and W. Wagner (2006), Evaluation of ERS scatterometer soil moisture products over a half-degree region in southwestern France, *Geophys. Res. Lett.*, vol. 33.

Shepard, D. (1968), A Two Dimensional Interpolation Function for Regularly Spaced Data, In Proceedings of National Conference of the Association for Computing Machinery, Princeton, NJ, USA, 1968; pp. 517-524.

SPOT Vegetation User's Guide, 2008: http://www.spot-vegetation.com/vegetationprogramme/Pages/TheVegetationSystem/userguide/userguide.html.

Teegavarapu, R. and V. Chandramouli (2005), Improved weighting methods, deterministic and stochastic data-driven models for estimation of missing precipitation records, *J. Hydrol.*, 312, 191–206.

Ulaby, F. T., A. K. Fung, and R. K. Moore (1981), Microwave and remote sensing active and passive, Norwood, MA: Artech House.

Ulaby, F. T., P. C. Dubois, and J. Van Zyl (1996), Radar mapping of surface soil moisture, *J. Hydrol.*, vol. 184(1/2), pp. 57–84.

Van Doninck, J., J. Peters, H. Lievens, B. De Baets, and N. E. C. Verhoest (2012), Accounting for seasonality in a soil moisture change detection algorithm for ASAR Wide Swath time series, *Hydrol. Earth Syst. Sci*., vol. 16, pp. 773–786.

Wagner, W. (1998), Soil Moisture Retrieval from ERS Scatterometer Data", PhD dissertation, Vienna University of Technology, Austria.

Wagner, W., G. Lemoine, and H. Rott (1999), A method for Estimating Soil Moisture from ERS Scatterometer and Soil Data, *Remote Sens. Environ*., vol. 70, pp. 191–207.

Wagner, W., C. Pathe, M. Doubkova, D. Sabe1, A. Bartsch, S. Hasenauer, G. Blöschl, K. Scipal, J. Martínez-Fernández and A. Löw (2008), Temporal Stability of Soil Moisture and Radar Backscatter Observed by the Advanced Synthetic Aperture Radar (ASAR), *Sensors,* vol. 8, pp. 1174-1197.

Zribi, M., A. Chahbi, Z. Lili, B. Duchemin, N. Baghdadi, R. Amri, A. Chehbouni (2011), Soil surface moisture estimation over a semi-arid region using ENVISAT ASAR radar data for soil evaporation evaluation, *Hydrol. Earth Syst. Sci*, vol. 15, pp. 345-358.

Zribi, M., C. André, B. Decharme (2008), A method for soil moisture estimation in Western Africa based on ERS Scatter meter, *IEEE Trans. Geosci. Remote Sens.*, 46, 2, 438-448.

Zribi, M., T. Paris Anguela, B. Duchemin, Z. Lili, W. Wagner, S. Hauesner, A. Chehbouni (2010), Analysis of relationship between soil moisture and vegetation in the Kairouan plain region of Tunisia using low spatial resolution satellite data, *Water Research Ressources*, VOL. 46, W06508, doi:10.1029/2009WR008196, 2010.

Figures and Tables

Table 1: Seasonal distribution of the radar image database
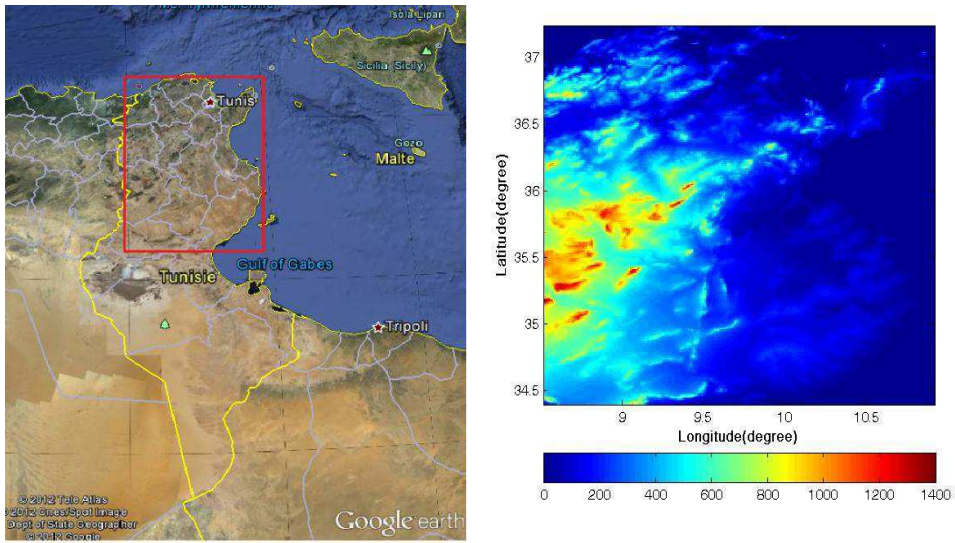
Figure 1: Map of the studied site and its corresponding DTM

Figure 2: Land use map

Figure 3: Maps of the β1, β2 and β3 slopes, used to normalize the backscattering coefficients for the three vegetation classes: (a) β1 for NDVI<0.25, (b) β2 for 0.25<NDVI<0.5, c) β3 for NDVI>0.5

Figure 4: Examples of radar data normalization for two different pixels: a) central Tunisia, characterized by class I and class II vegetation covers, and b) northern Tunisia, characterized by class II and class III vegetation covers.

Figure 5: In situ surface soil moisture measurements and precipitation recorded during the 2009-2011 period, on the Kairouan plain site.

Figure 6: Inter-comparison between the estimated soil moisture indexes proposed for ASAR WS data and ground moisture measurements

Figure 7: Inter-comparison between the ASAR WS index and the ASCAT/METOP (Vienna University) and ERS indexes, determined over the Kairouan plane.

Figure 8: Soil moisture index maps determined for different dates: a) 10/01/2006, b) 13/01/2009, c) 01/10/2009, d) 03/11/2010, e) 01/06/2011, f) 31/07/2011

Month	Number of ASAR images
January	22
February	12
March	15
April	15
May	5
June	10
July	14
August	11
September	10
October	16
November	13
December	8

Table 1: Seasonal distribution of the radar image database

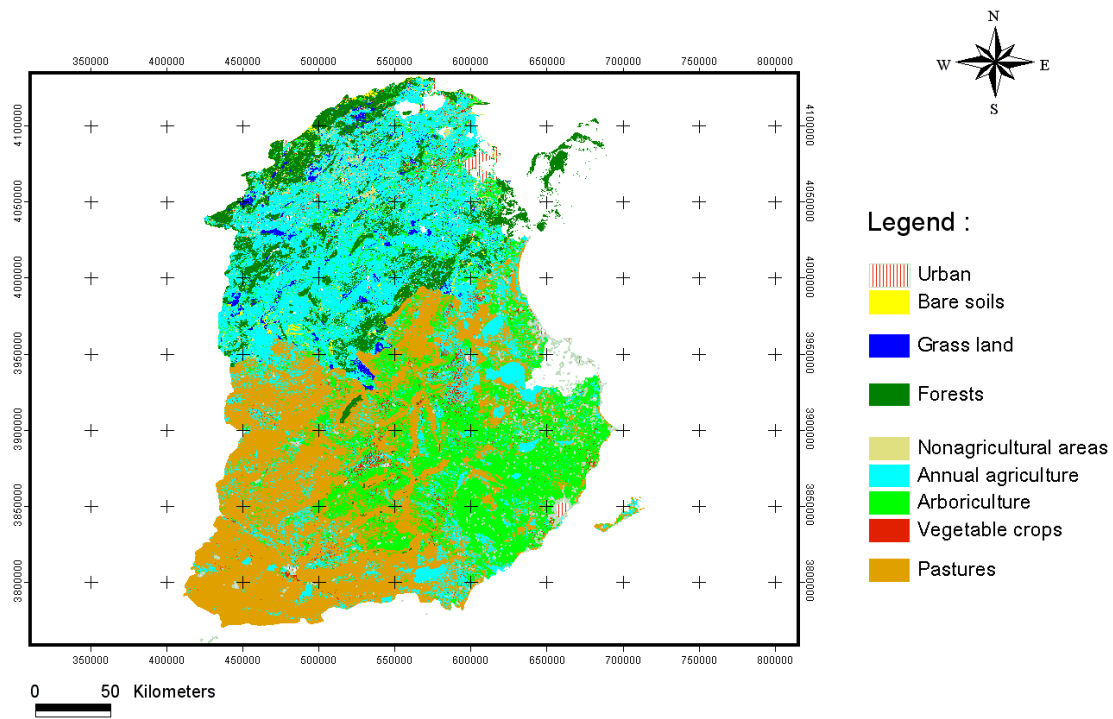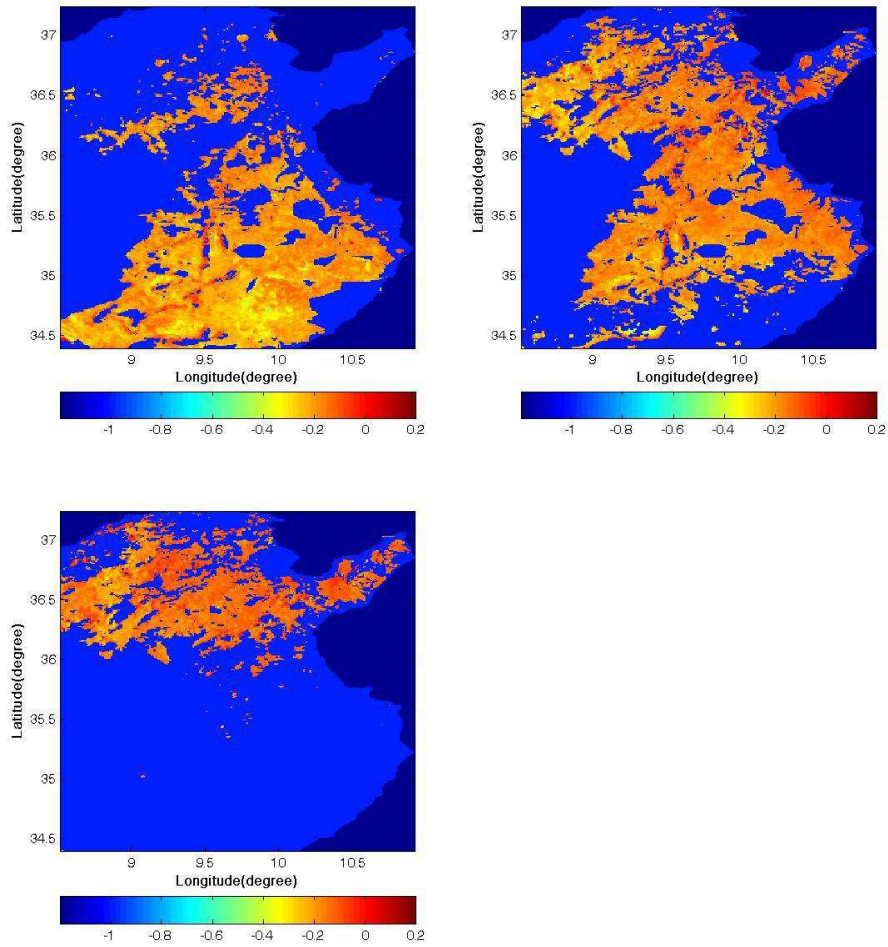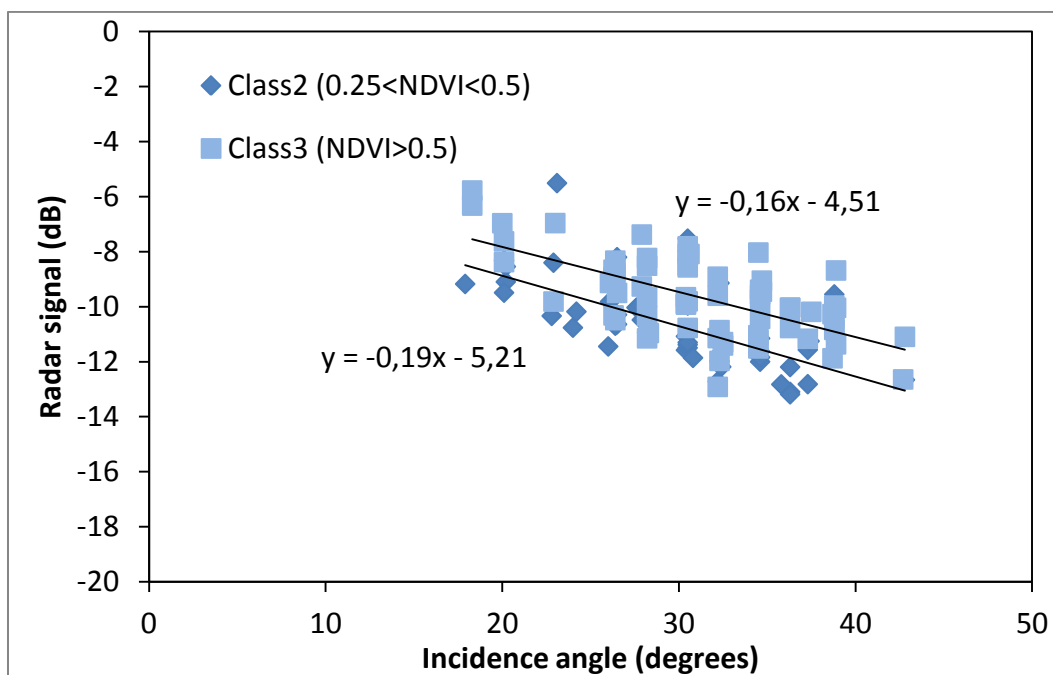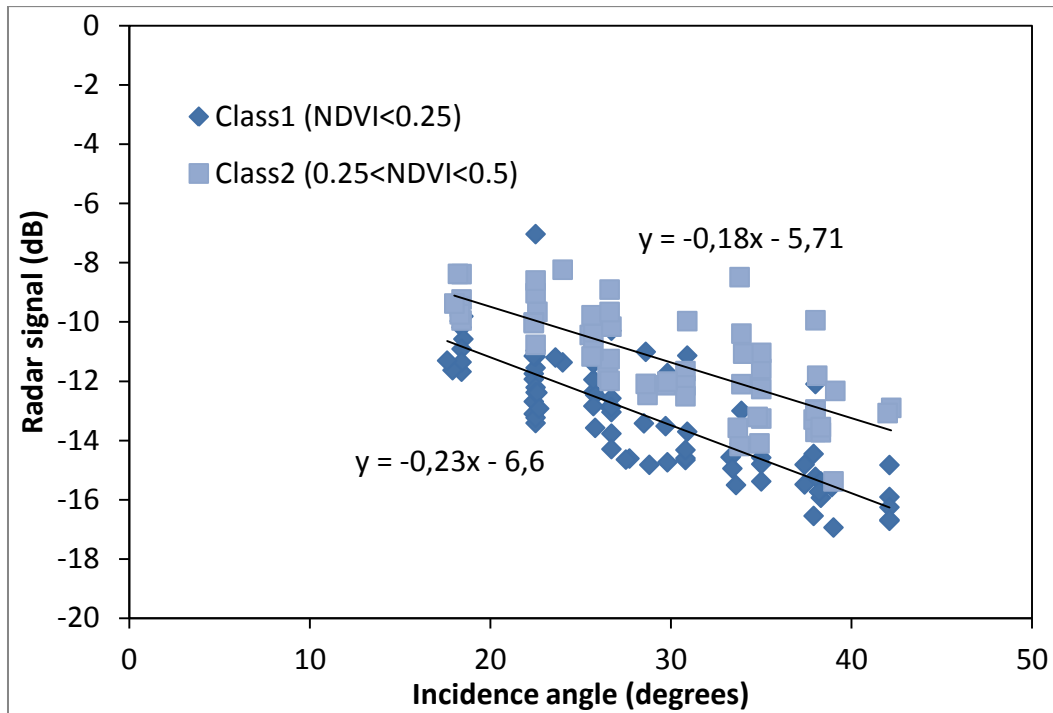Figure 1: Map of the studied site and its corresponding DTM

Figure 2: land use map

Figure 3: Maps of the β1, β2 and β3 slopes, used to normalize the backscattering coefficients for the three vegetation classes: (a) β1 for NDVI<0.25, (b) β2 for 0.25<NDVI<0.5, c) β3 for NDVI>0.5

Figure 4: Examples of radar data normalization for two different pixels: a) central Tunisia, characterized by class I and class II vegetation covers, and b) northern Tunisia, characterized by class I and class III vegetation covers.
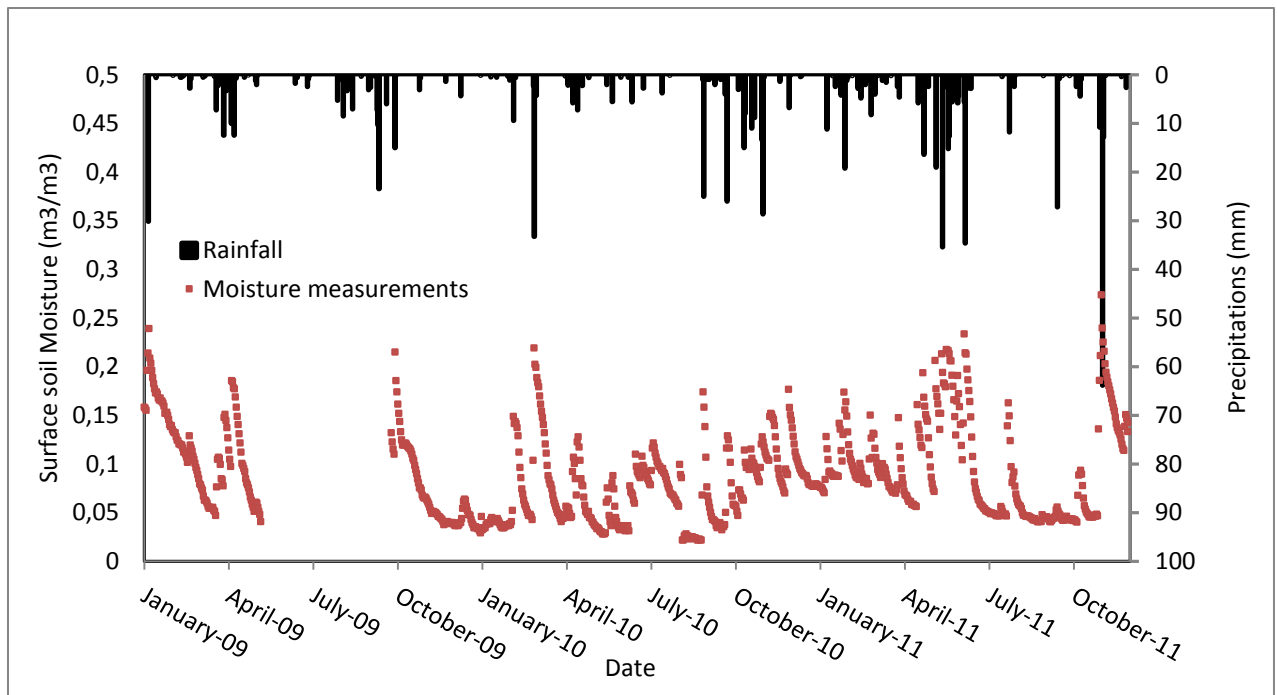
Figure 5: In situ surface soil moisture measurements and precipitation recorded during the 2009-2011 period, on the Kairouan plain site.

Figure 6: Inter-comparison between the estimated soil moisture indexes proposed for ASAR WS data and ground moisture measurements
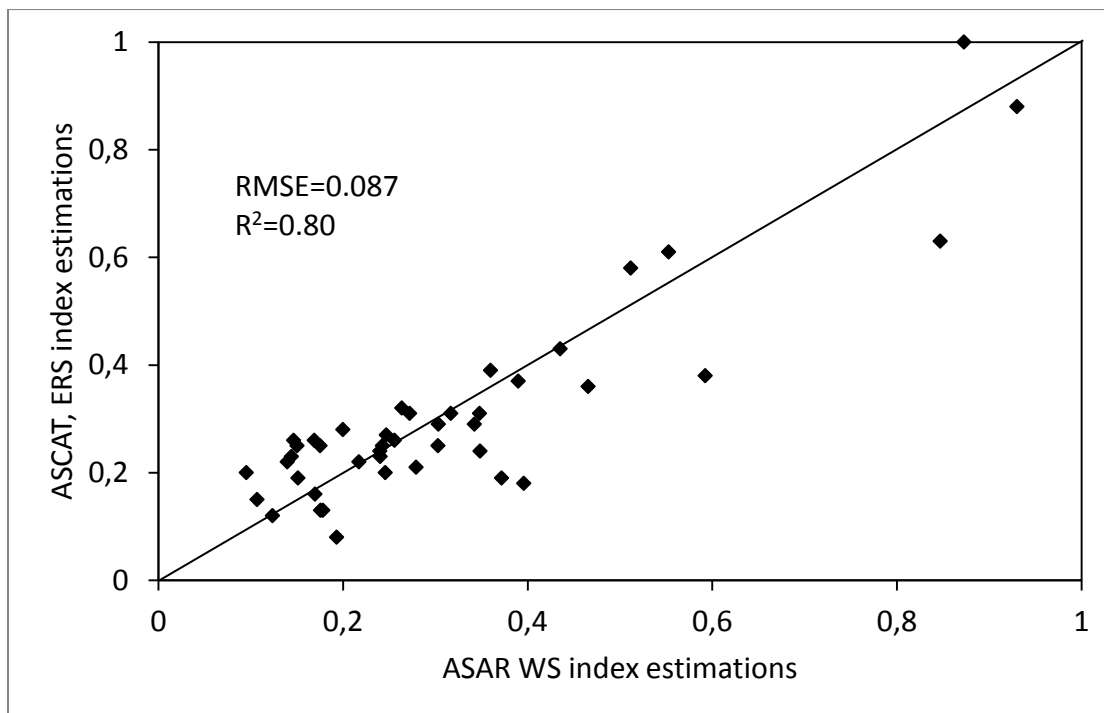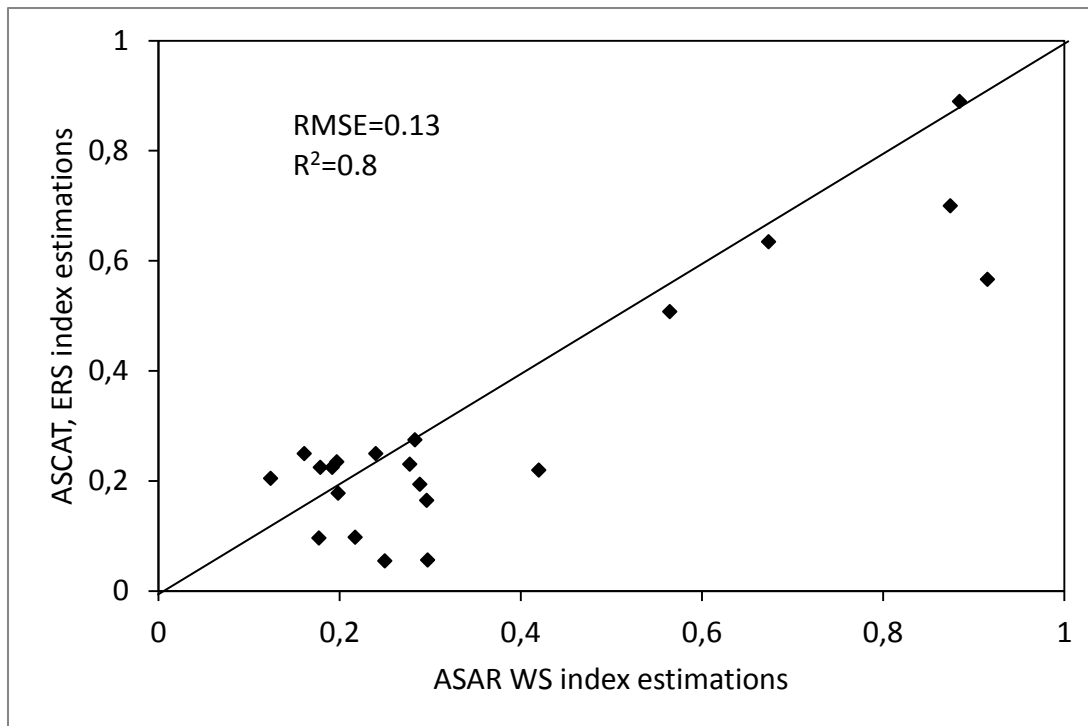
Figure 7: Inter-comparison between the ASAR WS index and the ASCAT/METOP (Vienna University) and ERS indexes, determined over the Kairouan plane, a) a pixel in the north of Kairouan plane, (b) a pixel in the south of Kairouan plane
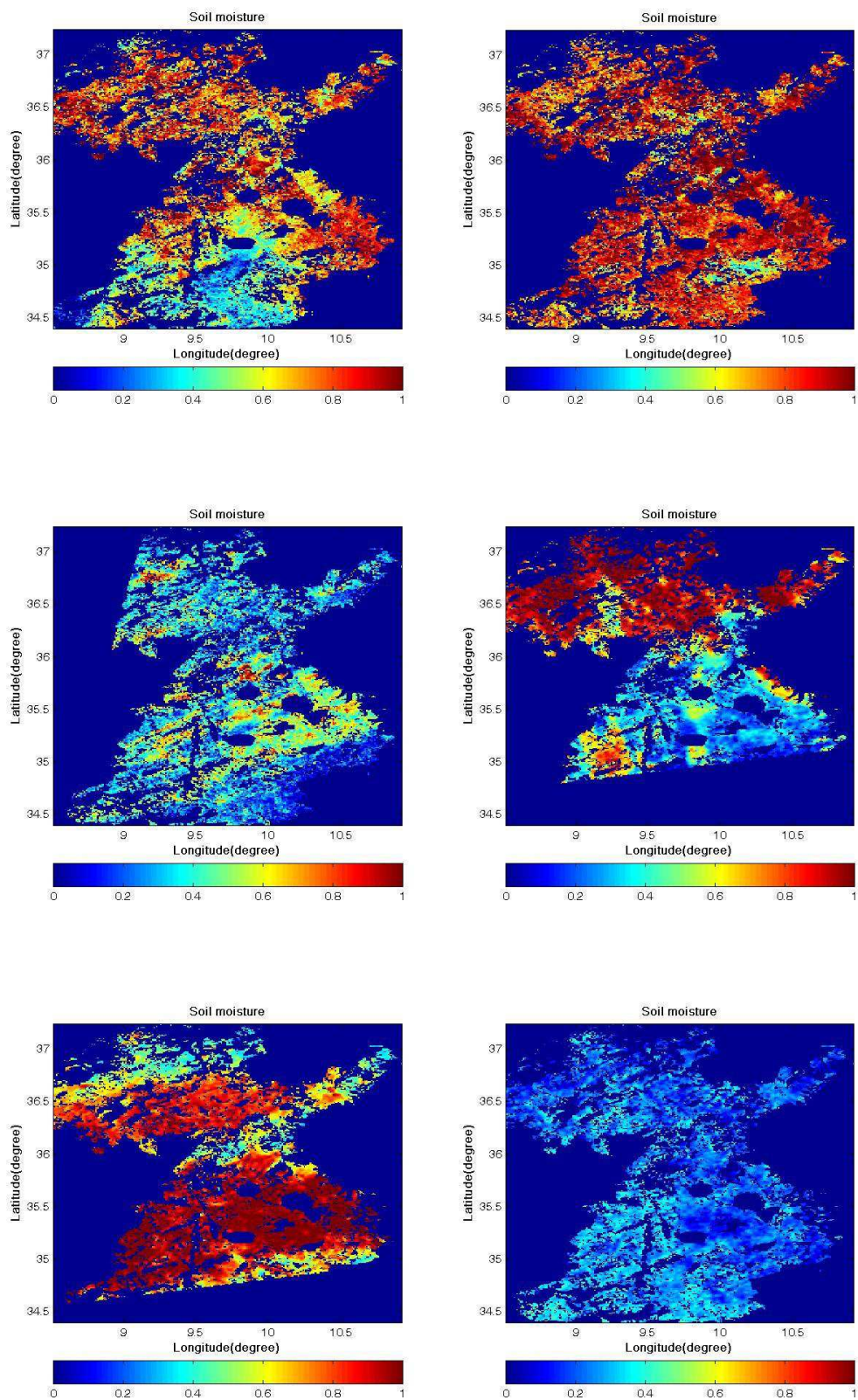
Figure 8: Soil moisture index maps determined for different dates: a) 10/01/2006, b) 13/01/2009, c) 01/10/2009, d) 03/11/2010, e) 01/06/2011, f) 31/07/2011